processes

MDPI

Article

Scenario-Driven Optimization Strategy for Energy Storage Configuration in High-Proportion Renewable Energy Power Systems

Hui Yang [1], Qine Liu [1,*], Kang Xiao [1], Long Guo [1], Lucheng Yang [1] and Hongbo Zou [2]

[1] State Grid Hubei Electric Power Co., Ltd., Xiangyang Power Supply Company, Xiangyang 441000, China; g28y0324@163.com (H.Y.); 13986318658@163.com (K.X.); hanyayishi86436@163.com (L.G.); 15623857213@163.com (L.Y.)

[2] College of Electrical Engineering and New Energy, China Three Gorges University, Yichang 443002, China; zhbhorace@ctgu.edu.cn

* Correspondence: lqekl@163.com

Abstract: The output of renewable energy sources is characterized by random fluctuations, and considering scenarios with a stochastic renewable energy output is of great significance for energy storage planning. Existing scenario generation methods based on random sampling fail to account for the volatility and temporal characteristics of renewable energy output. To enhance photovoltaic (PV) absorption capacity and reduce the cost of planning distributed PV and energy storage systems, a scenario-driven optimization configuration strategy for energy storage in high-proportion renewable energy power systems is proposed, incorporating demand-side response and bidirectional dynamic reconfiguration strategies into the planning model. Firstly, this paper designs a time series scenario generation method for renewable energy output based on a Deep Belief Network (DBN) to fully explore the characteristics of renewable energy output. Then, considering various cost factors of PV and energy storage, a capacity determination model is established by analyzing the relationship between annual planning costs, PV connection capacity, energy storage installation capacity, and power. Case studies are conducted on the IEEE-33 node system to compare and analyze the impact of active distribution network strategies on the planning results of PV and energy storage equipment under different scenarios. The results show that by incorporating demand-side response and bidirectional dynamic reconfiguration strategies into the active distribution network, the selection and sizing of PV energy storage can significantly improve the PV absorption capacity, achieve the lowest planning cost, and address the issue of low voltage levels during periods of excess PV output due to bidirectional reconfiguration. This improves the economic efficiency and reliability of the operation of power distribution networks with a high proportion of PV, providing a solution for energy storage planning that considers the randomness of renewable energy output.

Keywords: scenario-driven optimization; energy storage; renewable energy; deep belief network (DBN)

check for updates

Citation: Yang, H.; Liu, Q.; Xiao, K.; Guo, L.; Yang, L.; Zou, H. Scenario-Driven Optimization Strategy for Energy Storage Configuration in High-Proportion Renewable Energy Power Systems. *Processes* **2024**, *12*, 1721. https://doi.org/10.3390/pr12081721

Academic Editor: Masoud Soroush

Received: 1 July 2024
Revised: 28 July 2024
Accepted: 1 August 2024
Published: 16 August 2024

Copyright: © 2024 by the authors. Licensee MDPI, Basel, Switzerland. This article is an open access article distributed under the terms and conditions of the Creative Commons Attribution (CC BY) license (https://creativecommons.org/licenses/by/4.0/).

1. Introduction

China has established the "dual carbon" strategic goals of peaking carbon emissions by 2030 and achieving carbon neutrality by 2060. It is foreseeable that in the next 40 years, under the guidance of the "dual carbon" goals, China's energy and electricity supply system will undergo fundamental changes, and green and low-carbon energy, especially renewable energy generation, will become the mainstay of electricity production [1,2]. Renewable energy sources such as solar energy and wind energy have the advantages of clean, low-carbon, and abundant resources and wide distribution [3]. At the same time, they also have the disadvantages brought by natural attributes, such as low energy density and high volatility. Vigorously developing a long-distance transmission and distributed

power network infrastructure to enhance regional balances between power and load, and vigorously developing and mobilizing various flexible resources and energy storage options to achieve power and electricity balance, are important goals and essential requirements for the future development of new power systems [4].

In recent years, with the support of the state, local authorities, and power grid companies, energy storage ontology technology, integration technology, and application technology have been deeply studied, and many energy storage demonstration projects have been implemented [5]. On the basis of demonstration projects, extensive research has been conducted on the capacity allocation of energy storage in different application scenarios and functions, mainly including the following: the capacity allocation of energy storage in renewable energy generation systems under application functions such as stabilizing power fluctuations, reducing reserve capacity, reducing energy consumption, improving acceptance capacity and power prediction errors, etc.—such as improving the impact of high-permeability distributed photovoltaics on grid connection—reducing curtailment, reducing peak valley differences, peak shaving and valley filling, and improving power quality [6,7].

In terms of energy storage capacity, power configuration, and optimization of charging and discharging strategies, typical methods for configuring energy storage capacity primarily aim to establish mathematical models for optimizing energy storage capacity based on minimizing energy storage costs [8], maximizing benefits [9], maximizing return on investment [10], or minimizing capacity [11]. Reference [12] established a capacity allocation model that considers photovoltaic output fluctuations and the economics of energy storage users to determine the optimal energy storage capacity. However, it did not consider the optimization of battery power. Reference [13] established a mixed-integer linear programming (MILP) model aimed at reducing annual total costs, decoupling capacity optimization from operational optimization, thus reducing the complexity of the problem. In [14], a linear programming mathematical model for photovoltaic energy storage was established to optimize parameters. An optimal energy storage battery capacity and power were allocated with the goal of minimizing annual total costs. However, it did not consider the impact of battery capacity decay and battery cycle count on the system economics.

In recent years, due to improvements in the techno-economic level of some battery energy storage technologies and the introduction of subsidy policies, there has been a gradual trend towards the transition of energy storage from demonstration applications to commercial applications, with some quasi-commercial energy storage projects already in operation. The issue of energy storage capacity configuration is no longer solely based on technical or economic indicators, and the issue of considering multi-objective energy storage capacity configuration has received attention. Reference [15] used a bi-level programming approach to establish a capacity allocation and charging/discharging strategy model based on maximizing energy storage revenue. The optimal configuration of energy storage capacity and power were calculated through iterative computations of the two-level model, and particle swarm optimization was used for a simulation analysis of relevant cases. Reference [16] subdivided energy storage batteries into main batteries and backup batteries to optimize different application scenarios, fully considering factors such as grid electricity pricing systems, investment costs for energy storage, optimal scheduling schemes, and deviations in power load forecasting, with the aim of maximizing system revenue. Reference [17] proposed a multi-objective optimization model for energy storage configuration in industrial photovoltaic microgrids, aiming to maximize the utilization of photovoltaic power generation and achieve maximum annual net profits. However, none of the aforementioned references considered the impact of battery capacity decay on the economics of the energy storage system. Energy storage equipment is a one-time investment, but during the use of the battery, the increase in battery cycle count leads to intensified battery capacity decay, which is bound to affect subsequent power optimization configurations. Additionally, traditional energy storage configuration methods set the battery cycle count to a rated value, which does not yield optimal economic results. To

gain a better understanding, a table comparing energy storage planning and configuration models is provided in Table 1 below, in which the advantages and disadvantages of the current methods are detailed.

Table 1. Comparison of energy storage planning and configuration models.

References	Linear Model	Equipment Depreciation Loss	Voltage Instability Risk	Uncertainty of Renewable Energy	Network Loss
[8,12]	✔	×	×	×	✔
[13,14]	✔	✔	×	×	×
[15,16]	×	✔	×	✔	×
[17]	×	✔	×	✔	✔

On the other hand, the application scenarios and target models for grid-side energy storage are complex. Reference [18] conducted an analysis of the application value of typical energy storage cases in various grid-side application scenarios, including ensuring safety, enhancing transmission and distribution capabilities, reducing network losses, and improving the utilization level of renewable energy. Reference [19] used the Bayesian best–worst method and fuzzy cumulative prospect theory to form a multi-criteria group decision-making approach, enabling the selection and configuration of the optimal energy storage solution for specific application scenarios. Reference [20] established a techno-economic evaluation model for battery energy storage systems applied on the grid side, assessing the technical and economic feasibility of various solutions in four application scenarios. Reference [21] established a comprehensive evaluation system for the application of energy storage systems on the grid side, enabling the comparison of general characteristics with regional/technology-specific values to help identify overlapping areas between energy storage service requirements and storage capabilities, thereby selecting current and future grid-side energy storage systems. In anticipation of potential large-scale renewable energy cross-border grid energy storage application scenarios in the future, reference [22] established a multi-timescale energy storage capacity and location optimization analysis model, demonstrating through case studies that cross-border grid interconnection and renewable energy collaborative planning can effectively reduce energy storage installation capacity and lower system operating costs.

Under the requirement of promoting renewable energy consumption, reference [23] proposed an auxiliary decision-making method for grid-side energy storage configuration based on stochastic planning theory, quantifying the random scenarios of energy storage configuration under this demand and realizing an optimized grid-side energy storage configuration, which has a positive impact on improving the decision-making level of the grid-side energy storage configuration and promoting renewable energy consumption. Reference [24] proposed a joint optimization configuration of power to gas and multiple types of energy storage equipment to improve the system's capacity to absorb wind power. Reference [25] proposed a two-tier model for the optimized configuration of grid-side energy storage systems, considering multiple market-trading modes, aiming to maximize investment benefits and minimize system operating costs. Reference [26] considered system network structure constraints and conventional unit regulation capabilities, establishing a planning model aimed at minimizing energy storage capacity.

Although the aforementioned energy storage planning strategies have improved the economic efficiency of power system operation to a certain extent [27], there are still several issues that need to be addressed:

(1) The diverse and highly random nature of energy storage applications in the power system increases the complexity of planning. The rapid increase in the proportion of renewable energy sources such as wind and solar power, the rapid progress of terminal energy electrification substitution, changes in electricity consumption behavior brought about by electricity market reforms, the enhancement of source–grid–load coupling, and the

emergence of energy producers and consumers have all led to a rich and rapidly evolving range of energy storage application scenarios on the power supply side, grid side, and load side. This results in more complex and random/fuzzy factors in the basic data required for energy storage planning, making it more difficult to describe and characterize planning scenarios. This is a key technical issue that needs to be addressed first in energy storage planning research.

(2) The flexible operation modes and diverse mode combinations of energy storage have a significant impact on planning objectives. Multiple new energy storage technologies have the advantages of convenient deployment and flexible operation, and often provide multiple application functions in a specific scenario to achieve various planning objectives. To consider the effectiveness and benefits of actual operation during the planning stage, there is a need to tightly couple planning with operation. This involves addressing issues such as matching the long-term scale of energy storage planning and configuration with the short-term scale of operational benefits, nesting investment decision-making with operational verification, and effectively integrating the dominant factors of complex operational processes into the planning model.

2. Time Series Scenario Generation Method of Renewable Energy Output Based on Deep Belief Network

Utilizing artificial intelligence methods, black-box models are able to describe the randomness of renewable energy output without the need for the separate modeling of different renewable energy sources. Among these, unsupervised learning models represented by Deep Belief Networks (DBNs) have the advantage of strong learning capabilities and good adaptability. They can effectively fit the probability distributions of complex random variables, deeply explore various characteristics of benchmark data, and are suitable for the scenario generation of renewable energy output.

2.1. The Structure and Principles of Deep Belief Networks

A DBN is composed of multiple restricted Boltzmann machines (RBMs) connected in series. The learning and training process of a DBN typically consists of two stages: layer-wise pre-training and overall fine-tuning. The layer-wise pre-training is accomplished by training the RBMs. The specific structure and detailed principles of RBMs and DBNs are described as follows. The RBM is essentially an undirected graphical model, which consists of a visible layer $\boldsymbol{v}$ and a hidden layer $\boldsymbol{h}$. The random neurons in the two layers are represented by v_i and h_i, respectively, with biases a_i and b_i, respectively, where $a \in \mathbb{R}^n$, $b \in \mathbb{R}^m$. W represents the connection weights between the visible layer and the hidden layer, $W \in \mathbb{R}^{n \times m}$. The state variables of the random neurons in the two layers are binary, taking a value of 1 when activated and 0 when not activated. There are connections between neurons across layers but no connections within layers. By training the hidden units, the RBM can capture the correlation of the associated data expressed in the visible layer. The energy expression of an RBM can be defined in the following form:

$$F(v, h|\theta) = -\sum_{i=1}^{n} a_i v_i - \sum_{j=1}^{m} b_j h_j - \sum_{i=1}^{n} \sum_{j=1}^{m} W_{ij} v_i h_j \tag{1}$$

Here, $\theta = \{a, b, W\}$ represents the set of parameters for the RBM.

The joint probability distribution of the RBM is shown in the following Formula (2):

$$P(v, h|\theta) = \frac{e^{-F(v,h|\theta)}}{\sum\limits_{v,h} e^{-F(v,h|\theta)}} \tag{2}$$

The probability distribution of the visible units v can be further obtained as

$$P(v|\theta) = \frac{\sum_{h} e^{-F(v,h|\theta)}}{\sum_{v,h} e^{-F(v,h|\theta)}} \tag{3}$$

The visible layer and the hidden layer in the RBN are conditionally independent of each other. Therefore, the conditional probability distributions of the visible layer and the hidden layer are obtained as shown in Equations (4) and (5):

$$P(v|h,\theta) = \prod_{i=0}^{n} \frac{1}{(1+\exp(-W_i^T h - a_i))} \tag{4}$$

$$P(h|v,\theta) = \prod_{j=0}^{m} \frac{1}{(1+\exp(-W_j^T v - b_j))} \tag{5}$$

Using the maximum likelihood method to find the partial derivative of θ with respect to Equation (3), (6) can be obtained:

$$\begin{aligned} \frac{\partial \log P(v|\theta)}{\partial \theta} &= \frac{\partial \sum_{h} e^{-F(v,h|\theta)}}{\partial \theta} - \frac{\partial \sum_{v,h} e^{-F(v,h|\theta)}}{\partial \theta} \\ &= -\sum_{h} P(h|v,\theta) \frac{\partial F(v,h|\theta)}{\partial \theta} + \sum_{v,h} P(v,h|\theta) \frac{\partial F(v,h|\theta)}{\partial \theta} \end{aligned} \tag{6}$$

In the formula, [blank] represents the probability distribution of hidden units. Combining with the derivative of Equation (1), Equation (6) can be expressed in the following forms (7)–(9).

$$\frac{\partial \log P(v|\theta)}{\partial W_{ij}} = E(v_i h_j)_{P(h|v,\theta)} - E(v_i h_j)_{P(v,h|\theta)} \tag{7}$$

$$\frac{\partial \log P(v|\theta)}{\partial a_i} = E(v_i)_{P(h|v,\theta)} - E(v_i)_{P(v,h|\theta)} \tag{8}$$

$$\frac{\partial \log P(v|\theta)}{\partial h_{ij}} = E(h_j)_{P(h|v,\theta)} - E(h_j)_{P(v,h|\theta)} \tag{9}$$

Since there is currently no effective analytical calculation method for expectation $E(\cdot)_{P(v,h|\theta)}$, Gibbs sampling is usually used to approximate the log-likelihood probability. The parameter update formula is as follows:

$$\begin{cases} \Delta W_{ij} = \varepsilon(v_i^0 h_j^0 - v_i^k h_j^k) \\ \Delta a_i = \varepsilon(v_i^0 - v_i^k) \\ \Delta b_j = \varepsilon(h_j^0 - h_j^k) \end{cases} \tag{10}$$

In the formula, the superscript k represents the number of sampling iterations, and ε represents the learning rate. The DBN is a probabilistic generative model constructed by "stacking" several RBMs, where the hidden layer of one RBM serves as the visible layer of the next RBM. A typical DBN network architecture consists of several layers of RBMs and a logistic regression layer (usually a classifier), forming a deep neural network. Its structure is illustrated in Figure 1.

The training of the DBN is divided into two stages: layer-wise pre-training and overall fine-tuning. In the pre-training stage, training starts from the bottommost RBM, where the input data are the training data. The weights W_i and biases b_i of the RBM are first initialized, and then an unsupervised learning method is used to minimize the loss error of each RBM layer by layer, ensuring that as much feature information as possible is preserved

when mapping the feature data to different feature spaces. A logistic regression layer is set up in the final layer of the DBN, which receives the output feature data from the RBM as its input data. In the overall fine-tuning stage, a supervised learning method is used, and the labeled data are corrected through backpropagation and gradient descent to fine-tune the entire DBN network.

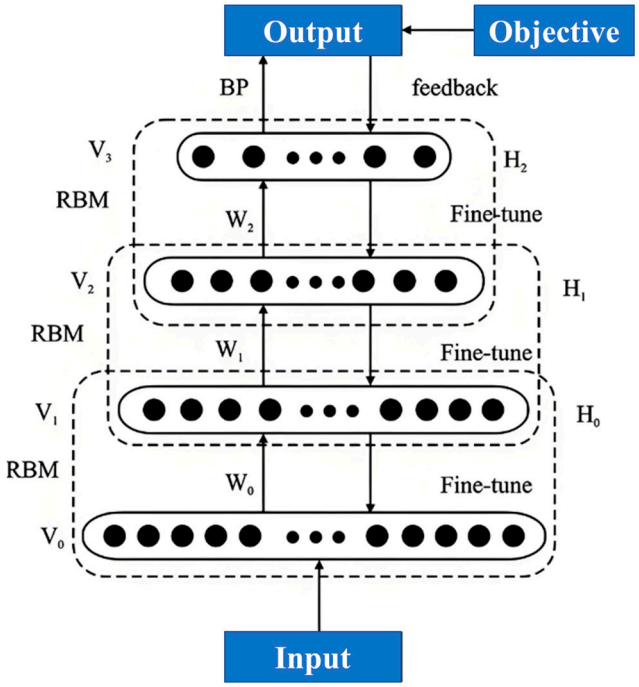

Figure 1. The structure diagram of a DBN model.

For each RBM, the iterative process between the hidden layer and the visible layer is carried out through Gibbs sampling to allow the weight parameters W_i to converge, ensuring that the training data in the hidden layer better approximate the distribution of the input data in the visible layer. Gibbs sampling is a special Markov Monte Carlo method that generates sample values for each attribute based on the conditional probability of one attribute, given the values of all other attributes in the sample.

2.2. Time Series Scenario Generation Method Based on Deep Belief Networks

To reveal the transition laws of the power generation state of renewable energy, Markov chains are adopted to describe the state of renewable energy output at each time step. First, let $Q(t)$ represent the output state of renewable energy at each moment, and divide the output state of renewable energy into N levels. The value range of $Q(t)$ is a positive integer between 1 and N, corresponding to the output state of renewable energy at time t, that is, $Q(t)$ has N states from "state 1" to "state N".

Based on the normalized data (ranging from 0 to 1) of the renewable energy output, the state is divided into N levels according to the output size, corresponding to N output states. Then, according to the statistics of the power generation states and their frequencies obtained from historical sequences, the Markov state transition probability matrix P_Q is calculated to describe the transition probabilities between adjacent states. The specific form is as follows:

$$P_Q = \begin{bmatrix} p_{11} & p_{12} & \cdots & p_{1N} \\ p_{21} & p_{22} & \cdots & p_{2N} \\ \vdots & \vdots & \ddots & \vdots \\ p_{N1} & p_{N2} & \cdots & p_{NN} \end{bmatrix} \tag{11}$$

The element p_{ij} represents the probability of the renewable energy output state transitioning from state i at time t to state j at time $t + 1$ (i, j = 1, 2, ..., N), and its specific form is

$$p_{ij} = P_r[Q(t + \Delta t) = j|Q(t) = i] \quad (12)$$

The formula with the $Pr()$ function is the probability calculation formula, which is used to calculate the probability of the renewable energy output state transitioning from state i at time t to state j at time $t + 1$.

The output state of the renewable energy undergoes transitions over time, and the cumulative state transition matrix generated by the Markov chain can describe the transition probabilities between different output states of the renewable energy. The historical sequence of renewable energy output is used as the input data for the DBN. Unsupervised layer-by-layer pre-training is performed from the bottom up, and after reaching the top layer, the backpropagation algorithm with gradient descent is used to correct the labeled data and fine-tune the entire DBN network. The data labels used in the backpropagation algorithm adopt the cumulative state transition probability matrix of the new energy output. This process of forward signal propagation and backward error propagation for weight adjustment in each layer is repeated continuously. The continuous process of weight adjustment is the learning and training process of the neural network. This process continues until the error of the network output is reduced to an acceptable level or until the preset number of learning iterations is reached. To gain a better understanding, the training process of a DBN involves the following steps:

1. Data Preprocessing: Firstly, extensive historical renewable energy output data are collected, typically including timestamps and corresponding output power values. These data undergo cleaning, to remove outliers and missing values, and necessary normalization to facilitate better learning by the model.
2. Constructing the DBN Structure: A DBN is a neural network composed of stacked layers of restricted Boltzmann machines (RBMs). Each RBM layer attempts to learn a higher-level abstract representation of the data. Based on the complexity of the problem and the characteristics of the data, structural parameters such as the number of layers in the DBN and the number of nodes per layer are determined.
3. Layer-wise Pre-Training: DBN employs unsupervised learning for layer-wise pre-training. Initially, the first RBM layer is trained to learn low-level features from the data. Then, the output of the first RBM is used as input for the second RBM, which is subsequently trained, and this process continues until all the layers have been pre-trained. This allows each layer to capture a portion of the data's features, laying a foundation for subsequent supervised training.
4. Fine-Tuning: After completing the layer-wise pre-training, the entire DBN network is unfolded into a feedforward neural network, and an output layer is added to generate time series scenarios. Supervised learning methods (e.g., a backpropagation algorithm) are applied to fine-tune the entire network, to minimize the error between the predicted and actual outputs. During fine-tuning, the pre-trained weights serve as initial values, accelerating the convergence process and enhancing the model's generalization ability.

Through its multi-layer structure, a DBN can learn complex nonlinear relationships within renewable energy output data. These relationships encompass the fluctuations in output power over time. During training, the DBN attempts to capture fluctuation patterns across different timescales, such as diurnal, weekly, and seasonal variations. By learning these patterns, the DBN can generate time series scenarios with similar fluctuation characteristics, simulating the uncertainty in renewable energy output. Each RBM layer in the DBN learns a portion of the temporal dependencies in the data. As the number of layers increases, the network is able to capture dependencies over longer time horizons. When generating time series scenarios, the DBN utilizes these learned temporal dependencies to predict future output values, considering not only current input conditions but also

historical temporal trends and periodic changes. Consequently, the generated scenarios effectively reflect the temporal characteristics of renewable energy output.

3. The Mathematical Model for Optimal Energy Storage Configuration

3.1. Introduction to Principles of Energy Storage Configuration

The primary research focus of this article is on the distribution network, where the renewable energy sources connected are primarily photovoltaic (PV). Wind power, which has a larger capacity, is often connected to the transmission network. Therefore, to better reflect reality, this article mainly considers the optimal configuration model for energy storage systems (ESSs) integrated with PV in the distribution network. When the PV output exceeds the total power supply load, the ESS absorbs the excess PV output, and the stored energy is preferentially released when the system voltage level is low. Assuming no energy losses during the charging and discharging of the ESS, and with a constant PV output, the total rated installed capacity of the ESS in the system is equal to the sum of the remaining PV output, which is the difference between the area of the PV output curve and the power supply load curve during the period of PV overproduction. In this case, there will be no redundant ESS capacity that would waste installation costs, nor will there be excess PV power fed back to the main grid. The total rated power of the ESS system is the maximum difference between the PV output curve and the power supply load curve during the period of PV overproduction. The configuration of the ESS is determined by the PV output curve and the total power supply load. The relationship is as follows:

$$p_{0,t} = p_{total,t} + p_{loss,t} \tag{13}$$

$$E_{ESS} = \begin{cases} \sum_{t=1}^{24} k_t |p_{PV,t} - p_{0,t}| & p_{PV,t} > p_{0,t} \\ 0 & p_{PV,t} \le p_{0,t} \end{cases} \tag{14}$$

$$p_{ESS} = \begin{cases} \max\limits_{t=1,2,\ldots,T} |p_{PV,t} - p_{0,t}| & p_{PV,t} > p_{0,t} \\ 0 & p_{PV,t} \le p_{0,t} \end{cases} \tag{15}$$

In the formula, $p_{0,t}$ represents the system power supply load at time (t); $p_{loss,t}$ represents the system network loss at time t; $p_{total,t}$ represents the user load at time t; E_{ESS} represents the rated installed capacity of the ESS; p_{ESS} represents the rated power of the ESS; and $p_{PV,t}$ represents the PV output at time t.

On the other hand, under the premise of high-proportion distributed PV integration into the grid and complete consumption of excess PV by the ESS, traditional energy storage optimization schemes aim to improve the PV consumption capacity by other means in the distribution network and reduce annual planning costs. The investment costs of the distributed PV and ESS are converted into annual equivalent costs, and the objective function is to minimize the annual planning costs, as shown in Equation (16):

$$\min C_{Total} = C_{INS} + C_{OM} + C_{buy} - C_S \tag{16}$$

Here, C_{Total} represents the annual planned cost for the system; C_{INS} stands for the equivalent annual installation cost; C_{OM} is the annual operation and maintenance cost; C_{buy} is the cost of purchasing electricity from the main grid; and C_S is the subsidy for photovoltaic power generation.

The annual installation cost of photovoltaic and energy storage devices can be calculated according to the following Formula (17):

$$C_{INS} = \frac{r(1+r)^{y_{PV}}}{(1+r)^{y_{PV}} - 1} c_{ins_PV} P_{PV} + \frac{r(1+r)^{y_{ESS}}}{(1+r)^{y_{ESS}} - 1} (c_{ins_ESS} E_{ESS} + c_{ins_pe} P_{ESS}) \tag{17}$$

Here, c_{ins_PV} represents the unit installation cost for PV systems; c_{ins_ESS} represents the unit installation cost for ESS (energy storage system) capacity; P_{PV} represents the total

installed power of distributed photovoltaic generation in the system; E_{ESS} represents the total installed capacity of ESS in the system; c_{ins_pe} represents the unit installation cost for ESS; P_{ESS} represents the total rated power of ESS in the system; y_{PV} represents the service life of distributed photovoltaic generation; and y_{ESS} represents the service life of ESS.

The annual operation and maintenance cost of PV and energy storage equipment can be calculated using the following Formula (18):

$$C_{OM} = \sum_{t=1}^{T} (c_{OM_PV} p_{PV,t} + c_{OM_ESS} \mu_{E,t} p_{ESS,t}) \tag{18}$$

Here, T represents the total annual hours, which is 8760 h; c_{OM_PV} represents the unit operation and maintenance cost of distributed photovoltaic power generation; c_{OM_ESS} represents the unit operation and maintenance cost of the ESS; and $\mu_{E,t}$ represents the charge/discharge flag of the ESS, where +1 indicates discharging, -1 indicates charging, and 0 indicates floating charge state.

The cost of purchasing electricity from the main grid can be calculated using the following Formula (19):

$$C_{buy} = \sum_{t=1}^{T} (p_{total,n} + p_{loss,n} - p_{pv,n}) \rho_{buy,n} \tag{19}$$

Here, $p_{total,n}$ represents the total user load on the n-th day; $p_{loss,n}$ represents the system line loss on the n-th day; $p_{pv,n}$ represents the total PV output on the n-th day; and $\rho_{buy,n}$ represents the electricity price of purchasing electricity from the main grid to the upper level on the n-th day.

The subsidy for power generation can be calculated according to the following Formula (20).

$$C_S = \sum_{n=1}^{365} a p_{pv,n} \tag{20}$$

Here, α represents the subsidy per unit of PV power generation.

Under the premise of known user load, the optimal configuration point of the ESS is determined by the rated installed capacity of distributed photovoltaic power generation. Ignoring the impact of distributed photovoltaic power generation and ESS connection locations on network loss changes, the annual total planning cost is related to the amount of distributed photovoltaic power generation connected. As the connected capacity of distributed photovoltaic power generation increases, the amount of electricity purchased from the upper grid decreases, but the installation and operation costs of distributed photovoltaic power generation and the ESS will increase. The relationship curve between the annual total planning cost and the connected capacity of distributed photovoltaic power generation exhibits a V-shape, reaching a minimum value at a certain point, achieving an optimal balance between the connected capacity of distributed photovoltaic power generation and planning costs. The rated capacity of distributed photovoltaic power generation at this minimum point is defined as the optimal rated installed capacity of the system, and the corresponding rated installed capacity of the ESS is also optimal, resulting in the lowest annual planning cost.

3.2. The Mathematical Model for Optimized Energy Storage Configuration

In this section, the mathematical model for optimized energy storage configuration is presented. For a distribution network, its structure can be altered, referred to as a distribution network reconfiguration. When the user load curve is changed through demand-side response strategies, or the network topology is modified through network reconfiguration, the minimum planning cost and its corresponding installed capacity of distributed photovoltaic power generation and ESS will also change. This paper proposes a photovoltaic and energy storage planning scheme that considers demand-side response

and bidirectional dynamic reconfiguration. A bi-level optimization model is established to obtain the optimal demand-side response strategy and dynamic reconfiguration strategy under different scenarios, thereby determining the user load curve, network topology, and final planning results for this active distribution network.

3.2.1. Upper-Level Model

The upper-level division model determines the division of peak and off-peak hours as well as the time-of-use electricity pricing. To achieve a closer alignment between user loads and photovoltaic output, and increase user loads during photovoltaic overproduction hours to absorb the excess photovoltaic power, the optimization of peak and off-peak hours division is conducted: Based on the characteristics of user loads and photovoltaic output on a typical day in a certain region, the period of photovoltaic overproduction is set as the off-peak hours, while the other periods are divided into peak and off-peak hours according to the original peak and off-peak characteristics.

Through the implementation of time-of-use electricity pricing strategy, the user loads during photovoltaic overproduction hours are increased, to absorb the excess photovoltaic power and reduce planning costs. The objective function of the upper-level division model is

$$f_1 = \min \frac{E_s}{E_0} \tag{21}$$

E_S represents the capacity of the ESS required after adopting a demand-side response strategy, while E_0 is the original installed capacity of the ESS. The smaller the ES is, the stronger the system's ability to absorb PV power becomes, and the lower the installation cost of the ESS will be.

(1) Demand Response-Related Load Constraints

Constraint (22) states that the total user load will remain unchanged before and after the implementation of demand response strategies.

$$\sum_{i=1}^{N} \sum_{t=1}^{24} p_{i,t} = \sum_{i=1}^{N} \sum_{t=1}^{24} p_{i,t}^{cur} \tag{22}$$

In the equation, $p_{i,t}$ and $p_{i,t}^{cur}$ represent the user load at node i before and after the implementation of time-of-use pricing at time t, respectively; N represents the total number of nodes in the system.

3.2.2. Lower-Level Model

We define the method of increasing system network losses by changing the network topology during periods of excessive photovoltaic output as reverse reconfiguration, which is used to absorb photovoltaic power. On the other hand, we define the method of reducing network losses during other periods as positive reconfiguration, aimed at reducing electricity purchase costs.

Based on the load characteristics and PV output characteristics of each period after the upper-level demand-side response, the optimal reconfiguration strategy is determined, including the number of reconfiguration periods and their division methods. The complex power of node N at time t is represented as $X_t = [x_{t1}, x_{t2}, \ldots, x_{tN}]$, and the daily system load is normalized and defined as $X = [X_1, X_2, \ldots, X_T]^T$. This matrix is then divided into time periods, where $1 \leq \alpha \leq \beta \leq N$, and the load segment difference within the period is $d_{\alpha\beta}$.

$$d_{\alpha\beta} = \ln \sum_{t=\alpha}^{\beta} \sum_{j=1}^{N} (x_{tj} - \overline{x}_j)^2 \tag{23}$$

$$\overline{x}_j = \frac{1}{\beta - \alpha + 1} \sum_{t=\alpha}^{\beta} x_{tj} \tag{24}$$

Assuming that S_d represents the sum of the load segment differences over m time periods, then

$$S_d^{(Y,m)} = \sum_{j=1}^{m} d_{i(j)+1,i(j)} \tag{25}$$

In the equation, Y represents the way that a typical 24 h daily cycle is divided into m reconfiguration periods. The greater the number of reconfigurations, the smaller the sum of segment differences, indicating that the data error within the periods of the reconfiguration division method Y is smaller. However, frequent reconfiguration can seriously affect the lifetime of switches, violating the constraint on the number of switch operations.

The objective function of the lower-level partitioning model aims to minimize the reconstruction error, i.e., to achieve a smaller sum of segment differences, while also reducing planning costs, under the constraint that the reconstruction frequency meets the required limitations. Since the two objective functions have different dimensions, they are normalized for comparison. The objective function of the lower-level partitioning model is

$$f_2 = \min\left\{ w_1 S_d^{(Y,m)} + w_2 \frac{C^{(Y,m)}}{C_0} \right\} \tag{26}$$

In the equation, $C^{(Y,m)}$ represents the annual planning cost of the network topology under the reconfiguration division method with m time periods and depreciation cost of the batteries, while C_0 stands for the original electricity purchase cost. Battery capacity degradation and cycle count both have significant economic impacts. As the battery capacity degrades, the overall performance of the energy storage system declines, potentially necessitating the early replacement of battery packs, thereby increasing replacement costs. Capacity degradation also leads to increased energy losses during charging and discharging processes, reducing the overall energy efficiency of the system. An uneven degradation of battery capacity can cause system performance instability, increasing failure rates and maintenance costs. The cycle life of batteries is limited, and with each completed charge–discharge cycle, the remaining life of the battery decreases. Therefore, the cycle count directly impacts the frequency and cost of battery replacements. As the number of cycles increases, the rate of battery performance degradation may accelerate, further exacerbating the economic burden. To account for this impact, the depreciation costs of batteries are considered in (26).

The following are the constraint conditions that need to be considered in the lower-level model.

(1) The reconfiguration of the distribution network should satisfy the following power flow constraints:

$$P_{G,i,t} - P_{L,i,t} = \sum_{j \in N(i)} |U_{i,t}||U_{j,t}||Y_{ij}| \cos(\theta_{ij} + \theta_{j,t} - \theta_{i,t}) \tag{27}$$

$$Q_{G,i,t} - Q_{L,i,t} = -\sum_{j \in N(i)} |U_{i,t}||U_{j,t}||Y_{ij}| \sin(\theta_{ij} + \theta_{j,t} - \theta_{i,t}) \tag{28}$$

In the equation, $P_{G,i,t}$ and $Q_{G,i,t}$ represent the active and reactive power injected by the power source at node i at time t, respectively; $P_{L,i,t}$ and $Q_{L,i,t}$ represent the active and reactive loads at node i at time t, respectively; Y_{ij} and θ_{ij} represent the conductance and conductance phase angle between nodes i and j; $U_{i,t}$ and $U_{j,t}$ represent the voltage magnitudes at nodes i and j at time t; and $\theta_{i,t}$ and $\theta_{j,t}$ represent the voltage phase angles at nodes i and j at time t, respectively.

(2) Voltage Amplitude Constraint

Changes in network losses will affect the voltage amplitude at each node. To ensure that the voltage level remains within the permissible range, it is necessary to meet the amplitude constraint.

$$U_{j,\min} < U_{j,t} < U_{j,\max} \tag{29}$$

In the equation, $U_{j,\max}$ and $U_{j,\min}$ represent the allowed upper and lower limits of the voltage, respectively.

(3) Constraint on the Number of Switching Operations

Frequent reconfiguration in the distribution network can reduce the lifetime of switches; thus, it is necessary to incorporate a constraint on the number of switching operations.

$$\sum_{q=1}^{Q} N_q \leq N_{\max} \tag{30}$$

In the equation, the 24 h cycle is divided into Q consecutive reconfiguration periods; N_q represents the number of switching operations within the q-th reconfiguration period. To achieve the efficient allocation of energy storage systems in distribution networks, this paper establishes a bi-level model. Solving bi-level optimization models is a complex process due to their nested structure and non-convexity, which increases the difficulty of finding solutions. Commonly used methods for solving bi-level optimization models include iterative methods, KKT condition transformation, extreme point search, and branch and bound methods. Iterative methods may not guarantee convergence to the global optimal solution, and for complex bi-level optimization problems, the iterative process can be time-consuming. As the problem size increases, the number of extreme points can grow rapidly, making extreme point search and branch and bound methods potentially infeasible. Therefore, this paper adopts the KKT condition transformation method [28], utilizing KKT conditions to convert the lower-level optimization problem into constraints for the upper-level optimization problem, thereby transforming the bi-level optimization problem into a single-level optimization problem. The specific steps are as follows: (1) Write out the KKT conditions for the lower-level optimization, including the gradient-equal-to-zero conditions, the complementary slackness conditions for inequality constraints, etc. (2) Incorporate the KKT conditions as constraints for the upper-level optimization—add the KKT conditions from the lower-level optimization to the upper-level optimization problem, forming a new single-level optimization problem. (3) Solve the single-level optimization problem—use existing optimization algorithms to solve the transformed single-level optimization problem.

4. Case Study

4.1. Introduction of the Testing System

Taking a 33-node distribution network system with an ESS (energy storage system) and distributed photovoltaic (PV) generation in a certain location as an example, the line voltage level is 12.66 kV. Its network topology is shown in Figure 2, where solid lines represent the original system branches, and dashed lines represent the tie switches that can be reconfigured. This paper does not consider the sale of electricity, and excess PV generation is fully absorbed by the ESS. The national PV subsidy reference is based on the 2023 national subsidy policy for PV generation, with a distributed electricity price subsidy standard of 0.42 yuan per kWh. According to the optimization model under the initial system, the relationship between the annual planning cost and the PV access capacity is determined, and the PV access capacity with the lowest cost is specified as the original PV access capacity, which is 2648 kW at this time. The installation location of the distributed PV is at node 3.

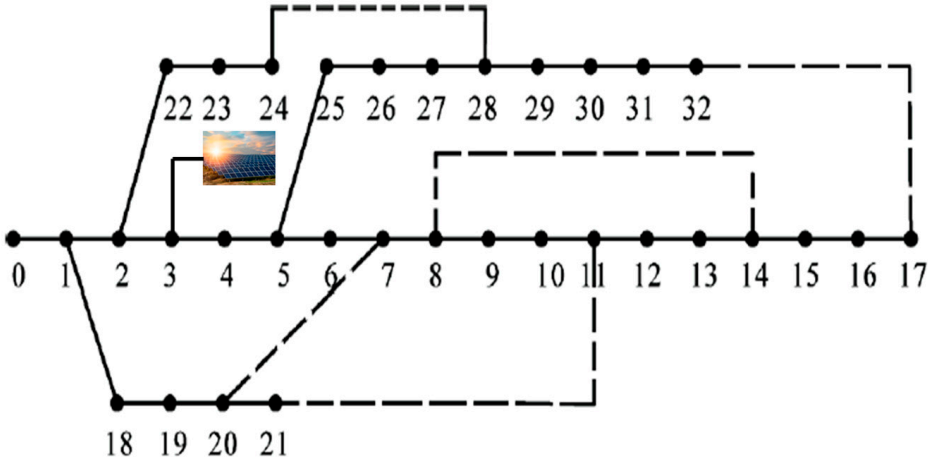

Figure 2. The structure diagram of IEEE-33 node testing system.

4.2. Effectiveness Verification of Scenario Generation Methods

To validate the superiority of the proposed DBN-based method for generating renewable energy output scenarios, the proposed method and the comparative MCMC method [11] were applied to generate renewable energy output scenarios using the above data. To more intuitively quantify the comparison results between the renewable energy historical sequences and the sequences generated by the two methods, the standard deviations of the wind power and PV sequence characteristic indicators were calculated separately, and the results are shown in Table 2. Standard deviation measures the dispersion of a set of data from its mean value, with a larger standard deviation indicating a greater difference between most values and their mean. Taking the historical sequence indicators as the benchmark, the closer the corresponding indicators of the generated sequence are to the historical sequence indicators, the more accurately the generated sequence can capture the characteristics of the historical sequence. As can be seen, the sequence indicators generated by the proposed method are closer to the historical sequence (with a smaller standard deviations for each indicator), indicating that the overall performance is superior to the MCMC method. Overall, compared to the MCMC method, the proposed renewable energy scenario generation method based on deep learning algorithms can better capture the characteristics of renewable energy output and is suitable for generating time series scenarios of renewable energy output.

Table 2. Comparison of renewable energy output sequence indicators.

Types of Renewable Energy	Different Methods	Monthly Standard Deviation	Daily Standard Deviation
Wind power	The MCMC method	0.0845	0.2456
	The proposed method	0.0654	0.2175
PV power	The MCMC method	0.1035	0.3154
	The proposed method	0.0895	0.2263

4.3. Time-of-Use (TOU) Electricity Pricing Period Division

First, the optimized division of peak and valley periods for time-of-use electricity pricing is determined, with the results shown in Figure 3.

Selecting a typical scenario under the current time-of-use electricity pricing information, the relevant scenario details are as follows. The user load and photovoltaic output during various time periods of a typical day are shown in Figure 4.

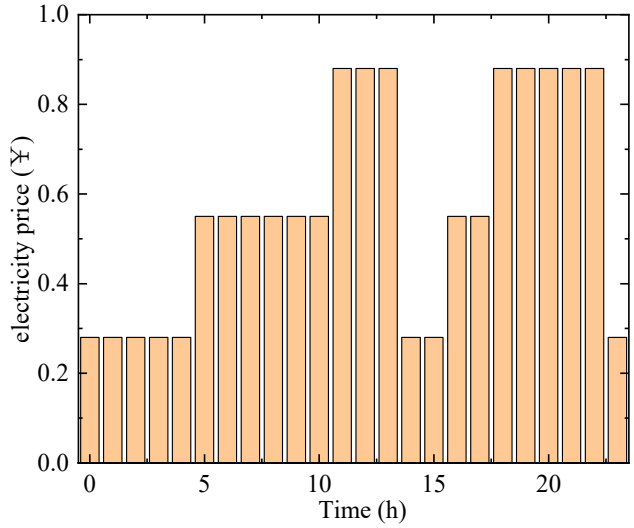

Figure 3. The optimized setting for time-of-use electricity pricing.

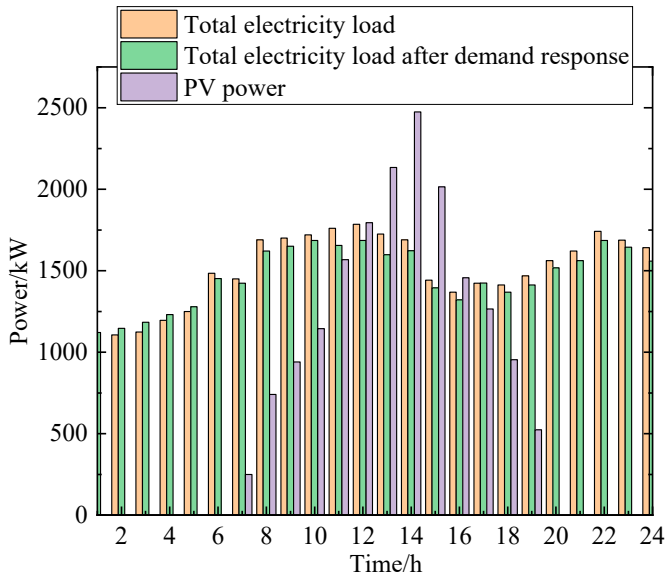

Figure 4. Load and photovoltaic output curve.

As can be seen from the graph, the period of excess photovoltaic output has become a valley period after the division of peak and valley periods. During this period, the electricity purchase price for users has decreased, leading to an increase in electricity consumption. Consequently, the total user load during this period has increased by approximately 7.4%. The excess photovoltaic output is absorbed by the ESS, and based on the optimization formula, the installation capacity of the ESS is determined. Compared to before implementing the demand-side response strategy, the demand for the ESS has decreased by approximately 32.4%, significantly enhancing the photovoltaic accommodation capacity. The load in other periods is shifted to the period of excess photovoltaic output, reducing the user load level.

On the other hand, a 24 h study period is divided into five consecutive restructuring periods, and the restructuring results are shown in Table 3. During the period of excess photovoltaic output, reverse restructuring is implemented to increase system network losses and accommodate photovoltaic output, thereby reducing the installation capacity and cost of the ESS. In other periods, forward restructuring is applied to reduce network losses, thereby lowering the electricity purchase cost.

Table 3. Results of dynamic reconfiguration considering demand response.

Interval of Reconfiguration Period		Action Switch
Forward reconfiguration	1:00–7:00 8:00–12:00	7-9-13-32-36 7-9-14-33-37
Reverse reconfiguration	13:00–15:00	2-11-15-33-35
Forward reconfiguration	16:00–21:00 22:00–24:00	7-9-14-17-27 7-9-11-33-37

4.4. Comparison and Analysis of Results from Different Planning Scenarios

By simulating the location and capacity determination of distributed photovoltaic power generation and the ESS in the following four scenarios, and comparing photovoltaic accommodation indices, annual comprehensive cost planning indices, voltage levels, and other indicators, the effectiveness and advantages of the proposed scheme were validated.

Scenario 1: Location and capacity determination are directly conducted without considering demand-side response and network reconfiguration.

Scenario 2: Location and capacity determination are conducted only considering bidirectional dynamic network reconfiguration, without considering demand-side response.

Scenario 3: Location and capacity determination are conducted only considering demand-side response, without considering bidirectional dynamic network reconfiguration.

Scenario 4: Location and capacity determination are conducted considering both demand-side response and bidirectional dynamic network reconfiguration.

Based on the initial capacity determination principles outlined in the first section, "distributed photovoltaic power generation output-annual planning cost" curves under different scenarios were plotted, and a comparative analysis was conducted on the annual planning costs and initial planning results for photovoltaic access capacity in each scenario, as shown in Figure 5. Taking Scenario 1, which does not adopt any active distribution network strategies, as the baseline, it is assumed that the distributed photovoltaic power generation and ESS are connected to each node evenly, ignoring the impact of network loss variations and node voltage level changes caused by different node access capacities. After considering only the bidirectional reconfiguration strategy or the demand-side response strategy, the lowest point of the cost curve shifts, with the planning cost at the lowest point dropping to 4.887 million yuan and 4.743 million yuan, respectively, and the photovoltaic access capacity increasing to 2321 kW and 2402 kW. Compared to other scenarios, the trough value of the cost curve in Scenario 4 further reduces the planning cost to 4.423 million yuan, and the corresponding rated installed capacity of distributed PV power generation increases to 2420 kW. This demonstrates that considering both demand-side response and bidirectional dynamic reconfiguration strategies has a positive impact on reducing planning costs and improving photovoltaic accommodation levels.

The active distribution network strategies in Scenarios 2, 3, and 4 all aim to enhance the PV accommodation level during periods of excess photovoltaic output, significantly reducing the installed capacity of the ESS to 425 kW, 375 kW, and 556 kW respectively. This leads to a decrease in the annual equivalent installation and operation and maintenance costs of the ESS. The planning results in each scenario show a slight increase in photovoltaic capacity, especially in Scenario 4, where the distributed photovoltaic generation capacity increases from the 2349 kW in Scenario 1 to 2458 kW. This increase in distributed PV generation capacity results in an increase in the annual equivalent installation and operation and maintenance costs. During periods of high photovoltaic penetration, excess distributed PV output is accommodated by the ESS and released during other periods of the day. The increase in PV output effectively reduces the system's electricity purchase costs and enhances PV subsidies.

To investigate the differences in node voltage levels under different scenarios, nodes 8 and 31, representing the lowest and highest load distributions in the system, were selected as typical cases for analysis. According to the PV output curve in Figure 3, the system's

photovoltaic integration is zero from 00:00 to 06:00 and from 20:00 to 24:00. Therefore, the differences in photovoltaic integration capacity between scenarios do not affect the node voltage levels during these periods.

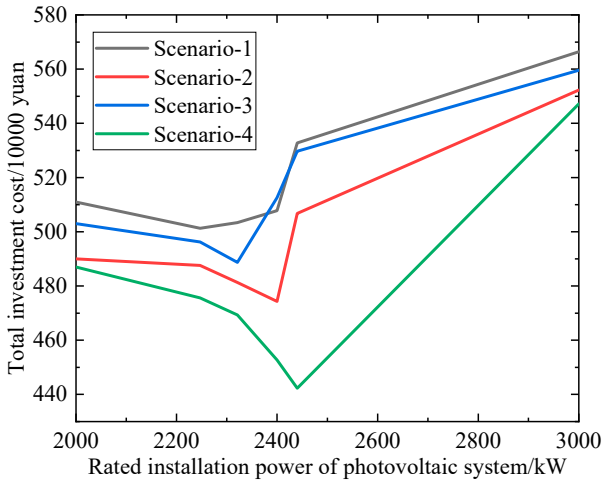

Figure 5. Total investment cost under different scenarios.

During periods of low solar irradiance, the voltage levels of both nodes in Scenarios 2 and 4 are similar to those in Scenario 1. However, in Scenario 3, the voltage levels of both nodes are improved due to forward reconfiguration, which reduces the network losses and optimizes voltage distribution, maintaining a high voltage level during this period.

During the period of high solar irradiance from 12:00 to 15:00, the voltage level in Scenario 2 is similar to that in Scenario 1. However, in Scenario 3, the voltage level drops significantly due to the increased network losses caused by reverse reconfiguration. The system's minimum node voltage is constrained to above 0.925 p.u. through voltage magnitude constraints. Scenario 4, which considers both demand-side response strategies and dynamic reconfiguration strategies, improves the voltage levels compared to the planning that only considers bidirectional reconfiguration strategies in the literature [17]. Specifically, the minimum voltage magnitudes of nodes 8 and 31 during this period increase from 0.947 p.u. and 0.938 p.u. to 0.993 p.u. and 0.992 p.u. respectively. This is because Scenario 4, after considering the demand-side response, improves the photovoltaic accommodation capacity. The photovoltaic integration capacity corresponding to the lowest cost point in this scenario increases by approximately 120 kW compared to Scenario 3, leading to a significant increase in photovoltaic output during this period and raising the node voltage levels within the system.

To further demonstrate the effectiveness of the method proposed in this paper, a comparison is made between the method presented here and those in references [13] and [15]. A unified DBN model is employed to generate typical scenarios, aiming to reduce the impact of scenario uncertainty. The relevant calculation results are shown in Table 4 below.

Table 4. Network loss and voltage magnitude comparison of different methods.

Methods	Network Loss/kW	Maximum Voltage Magnitude/p.u.	Minimum Voltage Magnitude/p.u.
The proposed method	2458.0	1.024	0.998
Method proposed in [13]	2562.3	1.035	0.985
Method proposed in [15]	2671.7	1.042	0.973

Upon observing the table above, it is evident that considering bidirectional power flow and demand response in the optimal allocation of energy storage in distribution networks can effectively reduce network losses and voltage fluctuations. Bidirectional power flow

allows energy to flow freely between the supply and demand sides in the distribution network, enabling energy storage systems to discharge energy during peak load periods, thereby alleviating the burden on the grid, and to absorb energy during off-peak periods, improving grid utilization. This flexible energy dispatch approach helps balance the supply and demand relationship of the grid, thereby reducing grid losses caused by mismatches between supply and demand. The introduction of energy storage systems can alter the power flow distribution in the distribution network. Through rational configuration and dispatch, it can reduce the reactive power flow in lines, decreasing network losses resulting from reactive power flow. Additionally, energy storage systems can serve as reactive power compensation devices, enhancing the power factor of the grid and further reducing network losses. Demand response incentivizes users to reduce power consumption during peak hours and increase it during off-peak hours, effectively balancing the load curve of the grid and reducing peak-to-valley differences. This load mitigation effect helps lower the risk of grid overload during peak periods, thereby reducing network losses and voltage fluctuations caused by overloading. As the proportion of renewable energy in the grid gradually increases, the instability of its output poses challenges to grid operation. Demand response can guide users to reduce power consumption during peak renewable energy output and increase it during troughs, smoothing out fluctuations in renewable energy output. This smoothing effect helps reduce voltage fluctuations and network losses arising from fluctuations in renewable energy output.

Another point that cannot be overlooked is that the scale of the testing system will also have an impact on the final results. This paper further employs the IEEE-69 and IEEE-123 node testing systems for verification. The topology of the testing systems is illustrated in Figure 6 below. The relevant computation time and network loss indicators are shown in Figure 7. The IEEE-33, IEEE-69 and IEEE-123 node testing systems are numbered 1, 2, and 3 respectively.

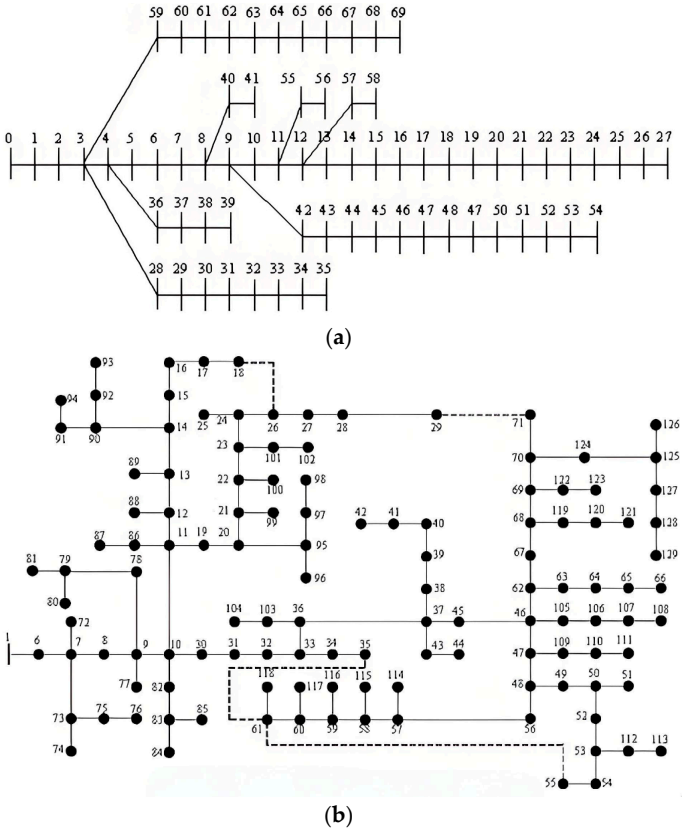

Figure 6. Topologies of testing systems with different scales. (**a**) Topology of IEEE-69 node testing system. (**b**) Topology of IEEE-123 node testing system.

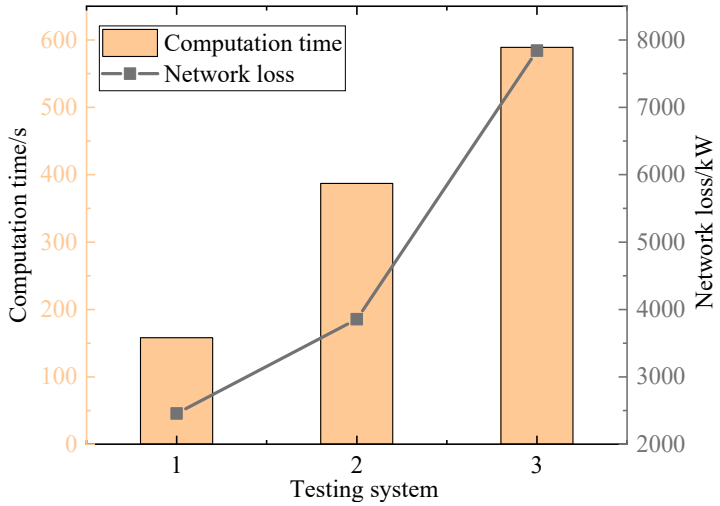

Figure 7. Computation time and network loss of testing systems with different scales.

By observing Figure 7, it can be seen that as the testing system scale increases, both the solution time and network losses also increase. Large-scale systems typically exhibit characteristics such as immense size, complex structures, diverse objectives, and numerous influencing factors. This necessitates that the energy storage configuration strategy fully considers the intricate relationships within the system and the interactions between different factors. Large-scale systems involve vast amounts of data, including real-time and historical data from various aspects such as power sources, loads, and energy storage. Processing these data requires significant computation time. Additionally, in large-scale systems, the economics of energy storage configuration become even more crucial. Due to the high investment costs associated with energy storage systems, it is imperative to minimize the configuration costs, while satisfying the demand. This requires the energy storage configuration model to comprehensively consider various economic factors (such as investment costs, operating costs, revenues, etc.) for economic evaluation.

5. Conclusions

This paper first generates scenarios for the long-term output of renewable energy. Through a two-layer partitioning model, an optimal demand-side response strategy and dynamic reconfiguration strategy are obtained. Based on this, the site selection and capacity determination are conducted, and a comparative analysis is made of the planning results for distributed photovoltaic power generation and an ESS under four scenarios. The following conclusions are drawn:

(1) A scenario generation method for renewable energy output time series based on Deep Belief Networks is proposed. Compared with the commonly used MCMC method, the proposed method can deeply explore the high-dimensional nonlinear characteristics of historical output sequences, accurately portraying the seasonality, volatility, and time-varying nature of renewable energy output.

(2) The segmented bidirectional dynamic reconfiguration strategy increases system network losses, to accommodate photovoltaic power during periods of excess photovoltaic output by performing reverse reconfiguration. This raises the system's electricity demand and demand for distributed photovoltaic power generation, but results in lower system voltage levels during these periods. When combined with a demand-side response strategy, the system connects to more photovoltaic sources, leading to increased photovoltaic output during these periods and achieving higher voltage levels.

(3) A distributed photovoltaic power generation and ESS planning that considers both demand-side response and bidirectional dynamic reconfiguration further reduces annual planning costs. Combining a network topology reconfiguration of the distribution network with time-of-use pricing strategies during periods of low photovoltaic penetration can

reduce system network losses and thus reduce electricity purchase costs. During periods of high photovoltaic penetration, reverse reconfiguration increases system network losses, and time-of-use pricing strategies encourage user consumption to increase the system load and accommodate more photovoltaic power, reducing electricity purchase costs and ESS demand.

Author Contributions: Conceptualization, H.Y., Q.L., K.X., L.G., L.Y. and H.Z.; methodology, H.Y., Q.L., K.X., L.G., L.Y. and H.Z.; software, H.Y., Q.L., K.X., L.G., L.Y. and H.Z.; validation, H.Y., Q.L., K.X., L.G., L.Y. and H.Z.; writing—original draft preparation, H.Y., Q.L., K.X., L.G., L.Y. and H.Z. All authors have read and agreed to the published version of the manuscript.

Funding: This research was funded by the State Grid Hubei Electric Power Co., Ltd. Technology Project: Research and Application of Key Technologies for Flexible Capacity Expansion of Distribution Networks Considering Mobile Energy Storage (No. 5215D0230003).

Data Availability Statement: The original contributions presented in the study are included in the article, further inquiries can be directed to the corresponding author.

Conflicts of Interest: Authors Hui Yang, Qine Liu, Kang Xiao, Long Guo and Lucheng Yang were employed by the company State Grid Hubei Electric Power Co., Ltd. The remaining authors declare that the research was conducted in the absence of any commercial or financial relationships that could be construed as a potential conflict of interest. The authors declare that this study received funding from State Grid Hubei Electric Power Co., Ltd.

References

1. Liu, X.; Liu, X.; Jiang, Y.; Zhang, T.; Hao, B. Photovoltaics and Energy Storage Integrated Flexible Direct Current Distribution Systems of Buildings: Definition, Technology Review, and Application. *CSEE J. Power Energy Syst.* **2023**, *9*, 829–845.
2. Qiu, D.; Chen, T.; Strbac, G.; Bu, S. Coordination for Multienergy Microgrids Using Multiagent Reinforcement Learning. *IEEE Trans. Ind. Inform.* **2023**, *19*, 5689–5700. [CrossRef]
3. Han, J.; Ji, X.; Feng, J.; Zhang, C.; Dehghanian, P.; Yang, D. Optimized Dispatch of Integrated Energy System with Hydrogen Energy and Carbon Capture Under Demand Side Response Mechanisms. In Proceedings of the 2023 3rd International Conference on Energy, Power and Electrical Engineering (EPEE), Wuhan, China, 15–17 September 2023; pp. 442–446.
4. Park, H.; Kim, M. Expected Benefits of Coordinated Energy Storage Operation in Stochastic Unit Commitment with Enhanced Deliverability of Reserves. *IEEE Access* **2024**, *12*, 18280–18294. [CrossRef]
5. Guo, S.; Kurban, A.; He, Y.; Wu, F.; Pei, H.; Song, G. Multi-Objective Sizing of Solar-Wind-Hydro Hybrid Power System with Doubled Energy Storages Under Optimal Coordinated Operational Strategy. *CSEE J. Power Energy Syst.* **2023**, *9*, 2144–2155.
6. Wu, X.; Liu, J.; Men, Y.; Chen, B.; Lu, X. Optimal Energy Storage System and Smart Switch Placement in Dynamic Microgrids With Applications to Marine Energy Integration. *IEEE Trans. Sustain. Energy* **2023**, *14*, 1205–1216. [CrossRef]
7. Wang, S.; Hui, H.; Ding, Y.; Ye, C.; Zheng, M. Operational Reliability Evaluation of Urban Multi-Energy Systems with Equivalent Energy Storage. *IEEE Trans. Ind. Appl.* **2023**, *59*, 2186–2201. [CrossRef]
8. Tan, X.; Wang, H.; Zhang, L.; Zou, L. Multi objective optimization configuration method and evaluation indicators for composite energy storage in microgrids. *Power Syst. Autom.* **2014**, 7–14. [CrossRef]
9. Xu, G.; Cheng, H.; Fang, S.; Ma, Z.; Zhang, J.; Zhu, Z. A battery energy storage configuration optimization model for improving the operational efficiency of wind farms. *Power Syst. Autom.* **2016**, *40*, 62–70.
10. Baghaee, H.R.; Mirsalim, M.; Gharehpetian, G.B. Multi-objective optimal power management and sizing of a reliable wind/PV microgrid with hydrogen energy storage using MOPSO. *J. Intell. Fuzzy Syst.* **2016**, *32*, 1753–1773. [CrossRef]
11. Lian, J.; Wang, D.; Yan, J.; Wang, K.; Cheng, S.; Jiang, K. Progress in Lead Carbon Battery Energy Storage Technology in the Field of Electric Power Storage. *Electr. Demand Side Manag.* **2017**, *3*, 21–25.
12. Xiong, X.; Ye, L.; Yang, R. Optimal Allocation and Economic Benefits Analysis of Energy Storage System on Power Demand Side. *Autom. Electr. Power Syst.* **2015**, *39*, 42–48.
13. Zhu, Q.; Li, Q.; Zhang, B.; Wang, L.; Li, G.; Wang, R. Capacity Optimization for Electrical and Thermal Energy Storage in Multi-energy Building Energy System. *Energy Procedia* **2019**, *158*, 6425–6430. [CrossRef]
14. Ni, C.; Liu, X. Battery capacity configuration and economic analysis of photovoltaic energy storage systems. *Zhejiang Electr. Power* **2019**, *38*, 1–10.
15. Zhu, J.; Liu, B.; Xie, H.; Li, H. User side energy storage capacity configuration and optimal operation strategy analysis based on two-layer programming. *South. Power Grid Technol.* **2016**, *10*, 43–50.
16. Li, Y. Research on Power Load Optimization and Dispatch Based on User Side Energy Storage System. Master's Thesis, Zhejiang University, Hangzhou, China, 2018.
17. Xu, J.; Liu, N.; Yu, L.; Lei, J.; Zhang, J. Optimization configuration of energy storage in industrial photovoltaic microgrids considering important loads. *Power Syst. Prot. Control* **2016**, *44*, 29–37.

18. Huang, B.; Hu, J.; Jiang, L.; Li, Q.; Feng, K.; Yuan, B. Application value assessment of grid side energy storage under typical scenarios in China. *Electr. Power* **2021**, *54*, 158–165.
19. Lu, H. Research on Energy Storage Plan Optimization and Comprehensive Value Measurement in the New Power System. Ph.D. Thesis, North China Electric Power University, Beijing, China, 2021.
20. Rahman, M.M.; Ahman, M.M.; Oni, A.O.; Gemechu, E.; Kumar, A. The development of techno-economic models for the assessment of utility-scale electro-chemical battery storage systems. *Appl. Energy* **2021**, *283*, 116343. [CrossRef]
21. Pearre, N.S.; Swan, L.G. Technoeconomic feasibility of grid storage: Mapping electrical services and energy storage technologies. *Appl. Energy* **2015**, *137*, 501–510. [CrossRef]
22. Jiang, H.; Du, E.; Jin, C.; Xiao, J.; Hou, J.; Zhang, N. Optimal planning of multi-time scale energy storage capacity of cross national interconnected power system with high proportion of clean energy. *Proc. CSEE* **2021**, *41*, 2101–2114.
23. Li, Z.; Yang, H.; Shi, T. Research on grid-side energy storage configuration based on stochastic programming theory. *Power Electron.* **2020**, *54*, 40–43.
24. Lu, B.; Wei, Z.; Wei, P.; Guo, Y.; Huang, Y.; Ma, X.; Zhou, F. Optimal configuration of P2G and energy storage equipment in regional integrated energy system considering wind power consumption. *Smart Power* **2021**, *49*, 7–14.
25. Wang, L.; Jiang, Y.; Wang, J. Optimization of grid-side energy storage considering multi-market transaction. *Power Syst. Clean Energy* **2020**, *36*, 30–38.
26. Yang, L.; Xu, Y.; Sun, H.; Wu, W. Tractable Convex Approximations for Distributionally Robust Joint Chance-Constrained Optimal Power Flow Under Uncertainty. *IEEE Trans. Power Syst.* **2022**, *37*, 1927–1941. [CrossRef]
27. Yang, L.; Xu, Y.; Zhou, J.; Sun, H. Distributionally Robust Frequency Constrained Scheduling for an Integrated Electricity-Gas System. *IEEE Trans. Smart Grid* **2022**, *13*, 2730–2743. [CrossRef]
28. Lu, Y.; Yu, X.; Jin, X.; Jia, H.; Mu, Y. Bi-Level Optimization Framework for Buildings to Heating Grid Integration in Integrated Community Energy Systems. *IEEE Trans. Sustain. Energy* **2021**, *12*, 860–873. [CrossRef]

Disclaimer/Publisher's Note: The statements, opinions and data contained in all publications are solely those of the individual author(s) and contributor(s) and not of MDPI and/or the editor(s). MDPI and/or the editor(s) disclaim responsibility for any injury to people or property resulting from any ideas, methods, instructions or products referred to in the content.